Shape-based Curve Growing Model and Adaptive Regularization for Pulmonary Fissure Segmentation in CT

Jingbin Wang[1], MEng, Margrit Betke[1], PhD, Jane P. Ko[2], MD

[1] Computer Science Department, Boston University, Boston MA 02215, USA
[2] Department of Radiology, New York University, New York NY 10016, USA
{jingbinw,betke}@cs.bu.edu

Abstract. This paper presents a shape-based curve growing model for object recognition in the field of medical imaging. The proposed curve growing process, modeled by a Bayesian network, is simultaneously influenced by the image data and knowledge of a prior curve shape. A maximum a posteriori (MAP) solution is derived by an energy-minimizing mechanism. It is implemented in an adaptive regularization framework which models the interaction between image data and shape prior influences and reflects the related causal dependencies in the Bayesian network. The method effectively alleviates over-smoothing, an effect that exists in other regularization methods. Moreover, the proposed framework also addresses initialization and local minima problems. Robustness and performance of the proposed method are demonstrated by segmentation of pulmonary fissures in computed tomography (CT) images.

1 Introduction

Enormous demands for automatically recognizing complicated anatomical structures in medical images have been raised in recent years. The medical community has seen many benefits from computer aided diagnosis (CAD) systems [5] and computer visualizations [6]. A large body of literature on segmentation of anatomical structures has been published [13]. Low-level image processing methods, such as thresholding or edge detection, by themselves, were often not sufficient for segmenting complete geometric structures of target objects. Many methods have attempted to introduce prior knowledge into the object recognition process by a model-based mechanism. A widely known technique, the "snake" or active contour method [7] used a deformable spline contour to capture the boundary of an object in an iterative energy minimizing process. The assumption of a smooth object boundary was guaranteed implicitly by the geometry of the spline contour. The level set method [11] was later proposed as a more powerful solution for handling instability and allowing changes in object topology. However, for objects with high curvatures or large boundary discontinuities, the smoothness assumption by itself is not sufficient for modeling object

shape. Thus, some high-level prior knowledge is needed to guide the object segmentation process. Statistics based methods (e.g., [4]) used training data for recognizing objects with complicated shapes. Recently several methods (e.g., [10]) have incorporated shape priors into existing segmentation methods, e.g., [7, 11], and presented promising results. In most applications, the above methods used closed contours to model objects. For an object modeled by an open contour, it is more appropriate to apply Berger and Mohr's method [1].

The main contributions of our paper are (1) a way to include a shape prior in a curve growing method for object segmentation (2) an adaptive regularization framework, (3) a way to address curve initialization and alleviate the local minima problem, (4) a successful application of the proposed method to the problem of segmenting fissures in CT. With the introduced shape prior, meaningful segmentation results are produced in the presence of uncertainties, such as ambiguous image features or high curvature variation on the object boundary. The adaptive regularization alleviates over-smoothing, an effect encountered by classical regularization methods. Our method also provides a solution for the initialization problem by taking advantage of the shape prior. It also alleviates the local minima problem effectively by a revised definition of the "image force." The performance of our method is evaluated in experiments on CT images for the specific application of pulmonary fissure segmentation.

2 Method

2.1 Bayesian Formulation of Curve Growing Behavior

Bayesian networks [12] have been applied to many applications that involve a reasoning process, as they succinctly describe causal dependencies using probabilities. Suppose that an object is modeled by a piecewise spline curve $\mathcal{C}$. A random variable I, representing the observed image data, and a random variable $\mathcal{C}^*$, representing prior information about the object shape, are considered as two causal predecessors of the random variable $\mathcal{C}$, the curve to be estimated. This relation can be modeled by the Bayesian network shown in Fig. 1A. The curve is represented as a collection of curve segments $\mathcal{C} = \{S_1, \ldots, S_K, \ldots, S_N\}$, where S_K represents the K-th curve segment and is also considered a random variable. The curve $\mathcal{C}$ is created by adding curve segments S_K one at a time. Random variable S_K is assumed to be only dependent on the most recently added curve segment S_{K-1} and not on earlier segments. We call this the "Markovianity assumption" [9] on subsequent curve segments. The corresponding Bayesian network is shown in Fig. 1B. Estimating the curve $\mathcal{C}$ is equivalent to finding the maximum of the joint probability $P(S_1, S_2, ..., S_N, \mathcal{C}^*, I)$ defined by the Bayesian network. By applying the Markovianity assumption, this is

$$P(S_1, ..., S_N, \mathcal{C}^*, I) = P(\mathcal{C}^*, I)P(S_1|\mathcal{C}^*, I)P(S_2|S_1, \mathcal{C}^*, I) \ldots P(S_N|S_{N-1}, \mathcal{C}^*, I). \quad (1)$$

This product includes the prior distribution $P(\mathcal{C}^*, I)$, which is generally assumed to be uniform, the posterior probability $P(S_1|\mathcal{C}^*, I)$, which models the probability

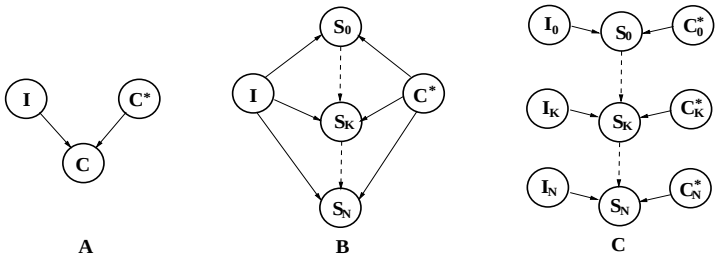

Fig. 1. A Hierarchy of Bayesian Networks for Curve Growing

of the initial curve placement and relates to the curve initialization problem, and the remaining posterior probabilities $P(S_K|S_{K-1}, \mathcal{C}^*, I)$, for $K = 1, \ldots N$. The maximum of the joint probability given in Eq. 1 is approximated by the product of the maximum of $P(S_1|\mathcal{C}^*, I)$ and each $P(S_K|S_{K-1}, \mathcal{C}^*, I)$, where

$$\begin{aligned} &P(S_K|S_{K-1}, \mathcal{C}^*, I) = P(S_K|S_{K-1}, \mathcal{C}^*_K, I_K) \\ &= P(I_K|S_K, S_{K-1}) P(\mathcal{C}^*|S_K, S_{K-1}, I_K) P(S_K, S_{K-1}) \,/\, P(S_{K-1}, \mathcal{C}^*, I_K). \end{aligned} \tag{2}$$

Here I_K is the local image region containing S_K and is considered to be the only relevant part of the image I for estimating S_K (Fig. 2). Similarly, $\mathcal{C}^*_K$ is the part of the shape prior $\mathcal{C}^*$ relevant to estimating S_K. The normalizing factor $P(S_{K-1}, \mathcal{C}^*, I_K)$ is considered irrelevant to S_K and omitted in its estimation. The corresponding Bayesian network is shown in Fig. 1C.

2.2 Energy Function of Curve Growing Model

The conditional probability $P(I_K|S_K, S_{K-1})$ in Eq. 2 is defined as:

$$P(I_K|S_K, S_{K-1}) \;\propto\; \exp(-|E_{img}(S_K) - E^{min}_{img}|\,), \tag{3}$$

where $E_{\text{img}}(S_K) = -\sum_i |\nabla I(V^i_K)|$ is the associated image energy of curve segment S_K, ∇I defines the image force, in many applications, the intensity gradient, V^i_K represents the i-th spline point in the segment S_K, and E^{min}_{img} is a lower bound on the values of E_{img} that can occur in an image. In contrast to previous methods [7, 16], the image energy is evaluated on the curve segment instead of a singular spline point, which reduces the possibility that the curve growing process is trapped in off-curve local image energy minima.

In Eq. 2, the probability $P(\mathcal{C}^*_K|S_K, S_{K-1}, I_K)$ is used for modeling the shape similarity between the current estimated curve C and the given shape prior $\mathcal{C}^*$. It is a function of S_K, S_{K-1} and I_K, and can be defined by a Gaussian distribution:

$$\begin{aligned} P(\mathcal{C}^*_K|S_K, S_{K-1}, I_K) \;&\propto\; \exp(-\alpha(I_K) f_{sim}(S_K, S_{K-1}, C^*_K)) \\ &= \exp(-|\mu(S_K, S^*_K) - \mu(S_{K-1}, S^*_{K-1})|/(2\sigma^2)) \text{ with} \\ \mu(S_K, S^*_K) = \tfrac{1}{n}\textstyle\sum_i |V^i_K - V^{i*}_K|,\; &S^*_K = \{V^{i*}_K | V^i_K \in S_K\}, \text{ and } C^*_K = S^*_K \cup S^*_{K-1}, \end{aligned} \tag{4}$$

where $f_{sim}(S_K, S_{K-1}, C_K^*)$ is a function measuring the similarity between (S_K, S_{K-1}) and the shape prior C_K^*, (V_K^i, V_K^{i*}) is a pair of corresponding points on $\mathcal{C}$ and $\mathcal{C}^*$ (correspondence is established by a closest point search [2]), $\mu(S_K, S_K^*)$ is the mean difference vector between two corresponding curve segments, n is the number of points included in S_K, and $\alpha(I_K)$ is a function of I_K used to control the magnitude of the Gaussian deviation ($\alpha(I_K) \propto 2\sigma^2$). Its main role will be discussed in next section.

The smoothness constraint on the curve is modeled by:

$$P(S_K, S_{K-1}) \propto \exp(-|f_{curv}(S_K, S_{K-1})|), \tag{5}$$

where $f_{curv}(S_K, S_{K-1})$ is a function measuring the curvature between S_{K-1} and S_K, e.g. as in Ref. [16]. By incorporating the Eqs. 3, 4, and 5 into Eq. 2 and taking the logarithm, the curve energy function

$$\begin{aligned}&\mathbf{E}(\mathcal{C}) = \mathbf{E}_{shape}(\mathcal{C}) + \mathbf{E}_{curv}(\mathcal{C}) + \mathbf{E}_{img}(\mathcal{C}) \;\propto \\ &\sum_{K=1}^{N} (\alpha_K(I_K) f_{sim}(S_K, S_{K-1}, C_K^*) + \beta_K f_{curv}(S_K, S_{K-1}) + \gamma_K E_{img}(S_K))\end{aligned} \tag{6}$$

is obtained, where α_K, β_K and γ_K are usually regarded as "regularization factors." Constraints on their ratios are relevant to the variances of the underlying Gaussian distributions. Each of E_{shape}, E_{curv} and E_{img} is normalized as suggested by Ref. [16]. The energy minimum of the function in Eq. 6 is considered an approximate MAP solution of the curve segmentation problem.

2.3 Causal Confidence Approximation and Adaptive Regularization

Ill-suited values for α_K, β_K and γ_K in Eq. 6 can cause the curve C to become overly smoothed due the shape prior or to include image clutter. Regularization factors can be estimated by different approaches, for instance, the cross-validation method [9], which, however, require a large amount of computation. To obtain a well-behaved regularizer, we propose an adaptive regularization

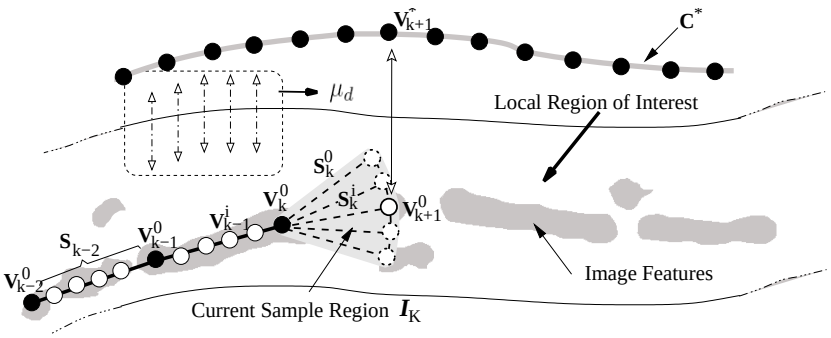

Fig. 2. Curve Growing with Adaptive Shape Influence

framework. A revised factor $\alpha(I_K)$ is introduced to model the dependency between I_K and the estimated S_K, which influences the belief represented by the distribution $P(\mathcal{C}^*|S_K, S_{K-1}, I_K)$. Such an adaptive behavior is directly related to the observed uncertainties of the image features, for which a common definition is the entropy [14], that is,

$$H(I_K) = -F \sum_{i=1}^{n} P(I_K|S_K^i, S_{K-1}) \log_2 P(I_K|S_K^i, S_{K-1}), \tag{7}$$

where S_K^i is the i-th sample of S_K in I_K, as illustrated in Fig. 2 and F is a normalizing factor. The entropy $H(I_K)$ can be interpreted as the amount of information contained in image region I_k. Based on $H(I_K)$, the parameter $\alpha(I_K)$ is then defined as

$$\alpha(I_K) \; = \; \max(\, \epsilon, \; (H(I_K) - \lambda)/(1 - \lambda)), \tag{8}$$

where λ is the threshold that corresponds to a desirable feature in I_K and can be learned offline from a set of training examples and where ϵ defines the minimum value of $\alpha(I_K)$. The values $\lambda = 0.5$ and $\epsilon = 0.1$ were chosen in the current implementation. Fig. 3(a)– 3(e) illustrates how the value of $\alpha(I)$ changes with regard to the image features along the curve. Fig. 3(f)– 3(i) shows a second example, where the curve segmented by the adaptive regularizer matches the ground-truth curve approximately, but the curve segmented by the static regularizer does not. In this case, the adaptive regularizer successfully weakened the influence of the prior shape, while in other cases, when the image region does not contain salient features, it strengthens it.

2.4 Curve Initialization

The curve growing process starts after a segment belonging to the curve is selected. The probability formulation $P(S_1|\mathcal{C}^*, I)$ suggests that both the shape prior C^* and the current image data I should be considered in this selection. In our work, the positions of salient image features, for example, local minima of the brightness gradient, are collected to form a set of candidate segments. Then, a confidence weight is assigned to each candidate segment. As an illustration, the dashed line L_i in Fig. 4(a) denotes the prior shape registered to the current segment S_i. Its confidence weight is calculated by accumulating the feature values along L_i in the image. The segment with the highest confidence weight among all segments is chosen as the initial curve segment. An example of the selection of an initial curve segment on CT is shown in Fig. 4(b). Our method provided more effective start conditions for the curve growing process than Berger and Mohr's method [1] for most of our data.

3 Results for Pulmonary Fissure Segmentation

A pulmonary fissure is a boundary between lung lobes which are distinct parts of the lung [8, 15, 17]. Its segmentation is of clinical interest because the fissure

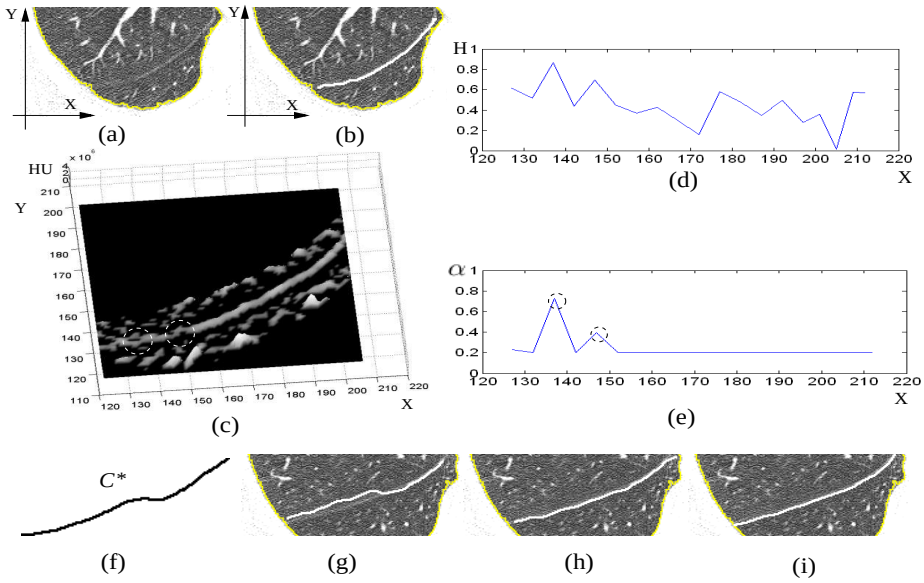

Fig. 3. Image features, entropy and adaptive regularization: Example 1: (a) Region of interest in a CT image. (b) Region with curve. (c) Feature map of region. (d) Value of entropy H along the curve. (e) Corresponding value of α. The two highest entropy values and the corresponding locations in the feature map are circled. Example 2: (f) Shape prior. (g) Curve obtained with static regularization, $\alpha = 1.2$ and $\gamma = 1.4$. (h) Curve obtained with adaptive regularization. (i) Ground truth curve.

can be used as cue to identify pulmonary nodules. On CT, a fissure often looks like a ribbon structure with variable width due to respiratory motion and the partial volume effect. In some slices, the fissure may appear as an incomplete curve composed of discontinuous segments. Tissue surrounding the fissure, e.g., adjacent vessels or nodules, and clutter due to noise in the imaging process can result in off-curve local minima of the image energy. Traditional active contour methods [7, 1] may not be able to overcome the above difficulties.

The proposed method has been tested to segment pulmonary fissures on 11 thin-section CT scans of 4 patients. On each slice, a morphological operation is applied to generate a feature map of the local region of interest containing the fissure. The prior shape C^* is estimated from fissures previously segmented in other images of the same scan. For each CT scan, the fissure on a single selected slice is segmented semi-automatically; the fissures on the remaining slices are then segmented fully automatically. The average time for segmenting fissures in one CT scan is less than 5 minutes on a PIII 1.2 GHz PC. Among 509 slices sampled from a total 1432 slices, the proposed method successfully segmented the fissures on 460 slices. The overall success rate of the method is 460/509=90.4%. The method then interpolated the segmentation of fissues on the remaining slices. Partial results are shown in Figs. 5 and 6 for illustration

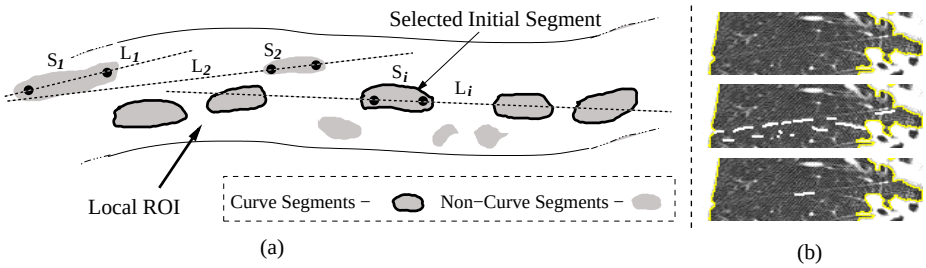

Fig. 4. Confidence weight of candidate segments: (a) Illustration of the confidence weight calculation. (b) A CT example with a local region of interest (top), candidate segments of collected features (middle), and the selected initial curve segment (bottom).

and comparison purposes. Berger and Mohr's method [1] produced comparable results in the few cases where image features are sufficiently salient. In many other cases, where image features are ambiguous, our method produced more meaningful results. Finally, the lung lobes were fully segmented by combining the segmented fissures with segmented lung contours [3], as visualized in Fig. 7.

4 Conclusion and Future Work

We described a shape-based curve-growing method and its application to pulmonary fissure segmentation. Selecting the location of the next curve segment in each iteration of the curve growning process effectively is a critical part of our solution. It overcomes some of the difficulties encountered by other methods [7, 1]. Moreover, the idea of adaptive regularization may be generalized and applied to many existing model-based energy-minimizing mechanisms. This will be investigated in future experiments involving different applications and higher dimensional spaces.

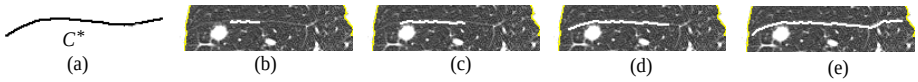

Fig. 5. A complete curve growing process:(a) the shape prior obtained from previous segmentations; (b) the found initial curve segment; from (c) to (e), the intermediate results after 4, 8, and 18 iterations, respectively.

References

1. M.O. Berger and R. Mohr. Towards autonomy in active contour models. In *Tenth International Conference on Pattern Recognition*, pp. 847–851, 1990.

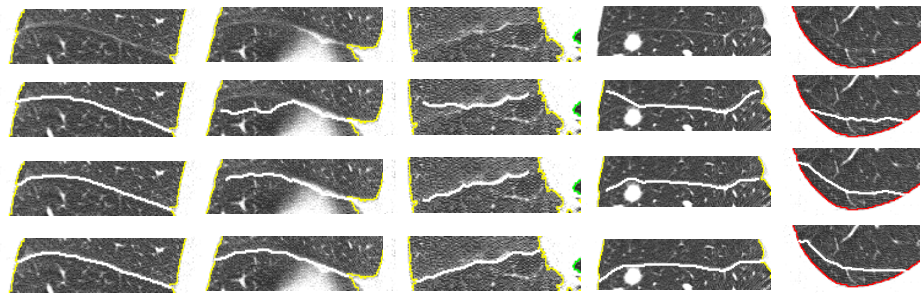

Fig. 6. Comparison of curve growing results: Row 1: Original images. Row 2: Curve by method in Ref. [1]. Row 3: Curve by current method. Row 4: Ground-truth curve, marked manually.

Fig. 7. Visualization of the segmented lung lobes of four patients.

2. P. J. Besl and N. D. McKay. A Method for Registration of 3-D Shapes. *IEEE Trans. Pattern Anal Mach Intell*, 14(2): 239–256, 1992.
3. M. Betke, J.B. Wang, and J.P. Ko. An intergrated chest CT image analysis system-"BU-MIA". *Tech. Report, Boston University, Computer Science Department*, 2003.
4. T.F. Cootes, C.J. Taylor, D.H. Cooper and J. Graham. Active shape models - their training and application. *Comput Vis Image Underst*, 61(1): 38–59, 1995.
5. M.L. Giger and C.J. Vyborny. CAD in mammography: rationale, methods and possible scenerios. *Diagnostic Imaging*, 98–113, Jun. 1993.
6. P. Golland, R. Kikinis, M. Halle, C. Umans, W.E.L. Grimson, M.E. Shenton, J.A. Richolt. AnatomyBrowser: A Novel Approach to Visualization and Integration of Medical Information. *J Computer Assisted Surg*, 4:129–143, 1999.
7. M. Kass, A. Witkin, and D. Terzopoulos. Snakes: Active contour models. *Int J Comput Vis*, 1:321–331, 1987.
8. M. Kubo, Y. Kawata, N. Niki et al.. Automatic extraction of pulmonary fissures from multidetector-row CT images In *Proceedings of the IEEE International Conference on Image Processing*. pp. 1091–1094, Greece, 2001.
9. S.Z. Li. Markov Random Field Modeling in Computer Vision. Springer-Verlag, 1995.
10. M.E. Leventon, W.E.L. Grimson, and O. Faugeras. Statistical shape influence in geodesic active contours. In *Proceedings of the IEEE Conference on Computer Vision and Pattern Recognition*, I:316–323, 2000.
11. R.Malladi, J.A. Sethian and B.C. Vemuri. Shape modelling with front propagation: A level set approach. In *IEEE Trans Pattern Anal Mach Intell*, 17(2): 158–175, 1995.
12. J. Pearl. Probabilistic reasoning in intelligent systems: Networks of plausible inference. San Mateo, Calif. Morgan Kaufmann, 1988.

13. D.L. Pham, C. Xu, and J.L. Prince. Current Methods in Medical Image Segmentation. *Annual Review of Biomedical Engineering*, 2, 2000.
14. C.E. Shannon. A mathematical theory of communication. *Bell System Technical Journal*, 27: 379–423, 623–656, 1948.
15. J. Wang, M. Betke, and J.P. Ko. Segmentation of pulmonary fissures on diagnostic CT – preliminary experience. In *Proceedings of the International Conference on Diagnostic Imaging and Analysis*, pp. 107–112, Shanghai, China, August 2002.
16. D.J. Williams and M. Shah. A fast algorithm for active contours and curvature estimation. *CVGIP: Image Understanding*, 55(1): 14–26, 1992.
17. L. Zhang. Atlas-driven lung lobe segmentation in volumetric X-ray CT images. Ph.D. Thesis, University of Iowa. 2002.